JOURNAL OF GEOPHYSICAL RESEARCH, VOL. 112, C11009, doi:10.1029/2007JC004189, 2007

Influence of (sub)mesoscale eddies on the soft-tissue carbon pump

Anne Willem Omta,[1] Bas Kooijman,[1] and Henk Dijkstra[2]

Received 27 February 2007; revised 30 July 2007; accepted 14 August 2007; published 14 November 2007.

[1] In an idealized situation of a baroclinically unstable single eddy, we study the impact of eddy-induced mixing on the soft-tissue carbon pump. The new element here is the coupling of a three-dimensional nonhydrostatic ocean model with a physiological plankton model that is able to represent a variable plankton C:N ratio. During the development and breakup of the eddy, a complicated vertical velocity field appears. The processes of transport and plankton growth, as well as the effect of the flow on the C:N ratio, are studied in detail. The physical processes associated with eddy breakup have a strong impact on the local environment in which the plankton grows. The changes in the local environment lead to a decrease of the C:N ratio (about 30% throughout the upper 150 m of the domain) and hence a weakening of the soft-tissue carbon pump. According to a sensitivity analysis, the decrease of the C:N ratio as a consequence of the flow field appears robust; it does not depend on specific parameter values in the model.

Citation: Omta, A. W., B. Kooijman, and H. Dijkstra (2007), Influence of (sub)mesoscale eddies on the soft-tissue carbon pump, *J. Geophys. Res.*, *112*, C11009, doi:10.1029/2007JC004189.

1. Introduction

[2] The marine biosphere is an important component in the global carbon cycle. Here the ocean circulation with all its variability interacts with marine life and its associated chemistry. One of the central processes is the biological carbon pump which involves gas exchange between the ocean and atmosphere, plankton dynamics and ocean mixing. It is crucial to understand the precise details of this pump, because the atmospheric carbon dioxide concentration is partially dependent on its strength.

[3] The soft-tissue carbon pump involves the sinking and subsequent remineralization of the 'soft' parts of algae. The 'hard' (i.e., carbonate and silicate) parts are involved in the so-called carbonate [*Volk and Hoffert*, 1985] and silicate [*Dugdale et al.*, 1995] pumps. The strength of the soft-tissue pump was defined by *Volk and Hoffert* [1985] as the difference in dissolved inorganic carbon (DIC) concentration between the surface and the deep ocean caused by the growth, sinking, and remineralization of algae. This difference is determined by R, the C:N (Redfield) ratio of the sinking organic material, and by ΔN, the difference in inorganic N concentration between the surface and the deep ocean [*Broecker*, 1982],

$$\Delta C = R\Delta N. \tag{1}$$

The C:N ratio R has been thought to be constant for a long time. In recent years, however, the uptake of C, N and P by oceanic biota has been observed to deviate strongly (up to 100%) from the classical Redfield C:N:P ratios at various locations on the ocean surface [*Sambrotto et al.*, 1993; *Emerson et al.*, 2001; *Karl et al.*, 2002]. An overview of the evidence for variability in the elemental composition of marine phytoplankton is given by *Geider and la Roche* [2002]. Using a mixed-layer model coupled to a physiological plankton model allowing for flexible plankton stoichiometry, *Omta et al.* [2006] have recently shown that external flow properties, such as the mixed-layer processes, can affect the algal C:N ratio and hence the soft-tissue carbon pump.

[4] As (sub)mesoscale flows are central in the upward transport of nutrients [*McGillicuddy et al.*, 1998; *Oschlies and Garçon*, 1998; *Martin and Richards*, 2001], a next important issue is the effect of these mesoscale flows on the soft-tissue carbon pump under flexible plankton stoichiometry. To understand these effects, we have chosen here a relatively simple (sub)mesoscale flow situation of a single initially cyclo-geostrophic eddy which is baroclinically unstable. Our study is more conceptual than site specific with DIN and DIC profiles typical of midlatitudes with the eddy simply providing a generic mesoscale ageostrophic circulation. An important advantage of our idealized flow structure over a baroclinically unstable jet generating a field of transient eddies as in, for example, work by *Lévy et al.* [2001] is that the developing vertical velocity field is dominated by a relatively simple flow structure. This makes it much easier to entangle causes and effects.

[5] In section 2, the biological model, the flow model and the initial conditions are described. Details of the coupled model and the numerical implementation are presented in Appendix A. Results on the flow patterns and the plankton and

[1] Institute for Molecular Cell Biology, Faculty of Earth and Life Sciences, Vrije Universiteit, Amsterdam, Netherlands.
[2] Institute for Marine and Atmospheric Research Utrecht (IMAU), Department of Physics and Astronomy, Universiteit Utrecht, Utrecht, Netherlands.

0148-0227/07/2007JC004189$09.00

Table 1. Hydrodynamic Model Parameter Values

Parameter	Interpretation	Units	Value
ρ_0	background water density	kg/m^3	10^3
T_0	water temperature at infinite depth	°C	5
$T_0 + T_1$	background surface water temperature	°C	8
ΔT	characteristic vertical temperature difference	°C	3
α	water expansion coefficient	°C^{-1}	10^{-5}
g	gravity acceleration	m/s^2	10
D_H	horizontal mixing coefficient	m^2/s	0.1
D_V	vertical mixing coefficient	m^2/s	10^{-5}
z_b	background vertical temperature decay depth	km	0.4
z_e	eddy decay depth	km	0.25
ΔT_e	maximum eddy temperature disturbance	°C	1.8
r_0	eddy radius	km	4
f_0	Coriolis parameter	s^{-1}	1.4×10^{-4}

nutrient distributions for a standard simulation and a number of sensitivity simulations are presented in section 3. The wider implications of these results are discussed in the last section.

2. Models and Methods

[6] We use a phytoplankton model coupled to a hydrodynamic model to simulate a phytoplankton population in a submesoscale eddy. The plankton model includes flexible stoichiometry; it is described in section 2.2 with details in Appendix A. The flow under consideration is a submesoscale vortex in which vertical transports are generated through baroclinic instability of the vortex itself. These vertical transports are very important for the plankton growth, because they bring nutrients to the euphotic zone and therefore it is crucial to simulate the vertical flow processes in a realistic fashion. For this reason, we use a nonhydrostatic three-dimensional hydrodynamic model [*Molemaker and Dijkstra*, 2000]. We simulate the flow in a horizontally square domain of length L = 32 km with a constant depth H of 1 km. We use Cartesian coordinates x, y, and z with $x = 0(L)$ at the western (eastern) boundary of the domain, $y = 0(L)$ at the southern (northern) boundary, $z = 0(-H)$ at the ocean-atmosphere (bottom) boundary. The flow model is briefly described in section 2.1 with the numerical details given by *Molemaker and Dijkstra* [2000]. The construction of the initial conditions is presented in section 2.3.

2.1. Flow Model

[7] The velocity field $\mathbf{u}$ and pressure field p are described by the three-dimensional Navier-Stokes equations and the continuity equation. The evolution of the temperature field T is described by an advection-diffusion equation. We assume a linear equation of state relating the density ρ to the temperature of the form $\rho = \rho_0(1 - \alpha(T - T_0))$ where ρ_0 and T_0 are reference values and α is the constant expansion coefficient. Using the Boussinesq approximation, the governing equations are

$$\frac{\partial \mathbf{u}}{\partial t} + (\mathbf{u}\cdot\nabla)\mathbf{u} + f_0\mathbf{e_z}\times\mathbf{u} = -\frac{1}{\rho_0}\nabla p + D_H\left(\frac{\partial^2}{\partial x^2}+\frac{\partial^2}{\partial y^2}\right)\mathbf{u} + D_V\frac{\partial^2\mathbf{u}}{\partial z^2} - \mathbf{e_z}\frac{g\rho}{\rho_0}, \quad (2)$$

$$\nabla\cdot\mathbf{u} = 0, \quad (3)$$

$$\frac{\partial T}{\partial t} + (\mathbf{u}\cdot\nabla)T = D_H\left(\frac{\partial^2}{\partial x^2}+\frac{\partial^2}{\partial y^2}\right)T + D_V\frac{\partial^2 T}{\partial z^2}, \quad (4)$$

where $\mathbf{e_z}$ is the unit vector in the vertical direction and g is the gravitational acceleration. The parameter values for the hydrodynamic model are given in Table 1 and below. At the lateral boundaries, periodic boundary conditions are applied. The boundary conditions at the top (z = 0) and bottom (z = −H) are

$$\frac{\partial T}{\partial z} = 0; \frac{\partial u}{\partial z} = 0; \frac{\partial v}{\partial z} = 0; w = 0. \quad (5)$$

The Coriolis parameter is constant throughout the domain at $f_0 = 10^{-4}$ s^{-1}. The parameters D_H and D_V are the horizontal and vertical mixing coefficients of both momentum and heat. We take D_H = 0.1 m^{2}s^{-1}, because dye release experiments [*Okubo*, 1971] suggest this value for the horizontal mixing coefficient at length scales of a few 100 m, i.e., the shortest scales that we resolve. We take $D_V = 1.0 \times 10^{-5}$ m^{2}s^{-1} which corresponds to vertical mixing by internal waves [*Wunsch and Ferrari*, 2004].

2.2. Plankton Model

[8] Because the strength of the soft-tissue carbon pump depends on the stoichiometry of the organic material sinking into the deep sea, we consider flexible stoichiometry as a necessary element of any biological model that is applied to represent the biological carbon pump. The primary mechanism known to cause variations in stoichiometry is found at the base of the foodweb: algae engage in luxury consumption, storing excess photosynthate (as starch or lipids) and nutrients (e.g., nitrate, phosphate) internally. This storage is particularly notable under limitation: nutrient-limited algae store high amounts of photosynthate derivates (leading to C:N ratios up to 28 [*Sterner and Elser*, 2002]), whereas light-limited phytoplankton can build up high-nutrient concentrations in vacuoles (leading to C:N ratios down to 4 [*Healey*, 1985]).

[9] In our Phytoplankton Internal Nitrogen and Carbon (PINC) model (inspired by the *Kooijman et al.* [2002] mixotroph model), algae consist of three components with different elemental compositions: organic structural mass (consisting of carbon and nitrogen in a fixed 10:1 ratio), an organic carbon reserve (consisting of carbon only), and a nitrogen reserve (consisting of nitrogen only). The ratios of these three components with respect to each other determine the C:N ratio of the organisms.

[10] The PINC model organism is schematically depicted in Figure 1. The organism produces nitrogen reserve (X_{E_N}) and carbohydrate reserve (X_{E_C}) by assimilating DIN (X_N) and DIC (X_C), respectively. The assimilation of DIC depends on the light intensity. The saturation constant for light $J_{L,FK}$ is equal to 25 mol/(m^2 d); the light flux $J_{L,F}$ (in mol/(m^2 d)) as a function of the vertical coordinate z is

$$J_{L,F} = 50e^{\frac{z}{d}}, \quad (6)$$

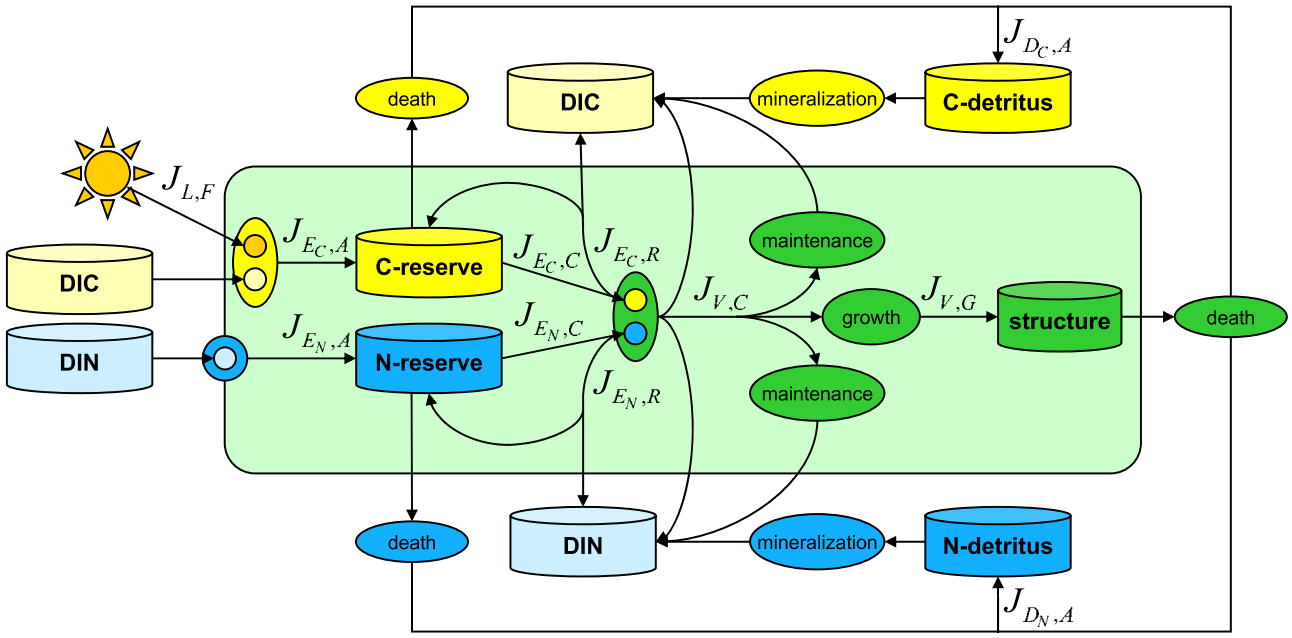

Figure 1. A schematic depiction of the PINC model; the model organisms need to take up DIC (X_C) together with light to form C-reserve (X_{E_C}), while no light is needed for the uptake of DIN (X_N) into N-reserve (X_{E_N}). The outflow from both reserves is combined in a fixed stoichiometry into a catabolic flux $J_{V,C}$ that is used for the maintenance and growth of the structure (X_V). The dead organic material is divided into N-detritus (X_{DN}) and C-detritus (X_{DC}) which remineralized into DIN and DIC, respectively.

with an extinction depth d of 14 m ($z = 0$ at the surface and $z = -H$ at the bottom). The assimilation fluxes of carbon and nitrogen into the reserves are denoted as $J_{E_C,A}$ and $J_{E_N,A}$. From the reserves, the catabolic fluxes $J_{E_C,C}$ (carbon) and $J_{E_N,C}$ (nitrogen) are mobilized to build structural biomass with a fixed C:N ratio of 10. If there is a 'mismatch' between the ratio of $J_{E_C,C}$ and $J_{E_N,C}$ and the C:N ratio of structure, then part of the carbon or the nitrogen flux cannot be used for structure synthesis and is therefore rejected. The flux of nonrejected material that can be used for metabolic processes is denoted $J_{V,C}$; the rejected fluxes of carbon and nitrogen are denoted as $J_{E_C,R}$ and $J_{E_N,R}$, respectively. A fixed fraction $0 < \kappa < 1$ of these rejected fluxes returns to the reserves, whereas the remaining fraction $1 - \kappa$ is exuded.

[11] The structural biomass requires maintenance, which is implemented as a fixed turnover rate k_M that returns to the dissolved inorganic matter pools. When maintenance has been 'paid', there remains a net growth rate which is denoted μ. Biomass (i.e., X_V, X_{E_C}, and X_{E_N}) turns into detritus at a death rate h_V. Because we are interested in the C:N ratio of this detritus, it is divided into a carbon component (X_{DC}) and a nitrogen component (X_{DN}). To close the carbon cycle, we impose a simple constant turnover of detritus h_D. This might be interpreted as remineralization of detritus by some constant background population of bacteria. The evolution of each biological field $X_i \in \{X_C, X_N, X_{E_C}, X_{E_N}, X_V, X_{DC}, X_{DN}\}$ is given by an advection-diffusion-reaction type equation,

$$\frac{\partial X_i}{\partial t} + (\mathbf{u}\cdot\nabla)X_i + w_S\frac{\partial X_i}{\partial z} = D_H\left(\frac{\partial^2}{\partial x^2}+\frac{\partial^2}{\partial y^2}\right)X_i + D_V\frac{\partial^2 X_i}{\partial z^2} + F_i, i = 1,\ldots,7, \quad (7)$$

with boundary conditions

$$\frac{\partial X_i}{\partial z} = 0, i = 1,\ldots,7 \quad (8)$$

at top and bottom of the domain and periodic conditions at the lateral boundaries.The biological fluxes F_i, i = 1, ..., 7 are the righthand sides of the equations (A8a) through (A8g), given in Appendix A. All the tracers are advected by the flow; detritus (X_{DC} and X_{DN}) is also advected as a consequence of sinking, i.e., $w_S = 0$ m/day for X_C, X_N, X_V, X_{EC}, and X_{EN}, $w_S = -10$ m/day for X_{DC} and X_{DN}. The equations for the biological quantities require a sophisticated advection scheme to prevent the occurrence of negative concentrations. We have used a third order upwind scheme with limiter [*Hundsdorfer and Verwer*, 2003] for the advection of the biological tracers. This scheme guarantees positive definite advection.

[12] Different phytoplankton species have different uptake affinities for nitrogen, carbon, light and they have different death and growth rates, etc. There may also exist an interspecies variation in the C:N ratio of biomass structure. Within one species, there is also a large spread between individuals, especially if these individuals live under different environmental conditions. Hence there exists a large spread in the possible values of the PINC parameters. To obtain an indication how sensitive the model predictions are to the values of the various parameters, we have performed the following study. First, we have made an estimate of the possible range in each of the parameter values. Then we have varied each parameter within its range in a zero-dimensional setup; that is, we have integrated the equations $\frac{\partial X_i}{\partial t} = F_i$ until equilibrium was reached. Because

Table 2. PINC Model Organism Parameter Values With Results From a Sensitivity Study[a]

Parameter	Interpretation	Units	Standard Value Parameter	Range Parameter	Range C:N
$n_{N,V}$	N:C of structure	mol N/mol C	0.1	0.05–0.3	4.2–22
$j_{EC,Am}$	max. C uptake	d^{-1}	2.5	0.25–10	0–35
$j_{EN,Am}$	max. N uptake	mol N/(mol C d)	0.25	0.025–1.0	9.9–12.6
K_C	sat. const. C upt.	μM C	500	50–5000	10.9–11.9
$J_{L,FK}$	sat. light flux	mol/(m^2 d)	25	2.5–100	0–32
K_N	sat. const. N upt.	μM N	0.1	0.01–1.0	11.8–11.8
$y_{E_C,V}$	yield factor C	–	1.5	1–3	0–13.9
$y_{E_N,V}$	yield factor N	mol N/mol C	0.15	0.10–0.30	11.1–12.4
k_E	reserve turnover	d^{-1}	4	1–16	10.6–12.4
k_M	maintenance rate	d^{-1}	0.1	0.01–0.3	0–14.7
h_V	death rate	d^{-1}	0.1	0.03–0.3	0–14.7
κ	damming up fr.	–	0.9	0–0.999	9.7–18.9
h_D	detritus decay	d^{-1}	0.5	0.01–1.0	11.8–11.8

[a]For each of the parameters, we have estimated a range of possible values (fifth column). We have varied the parameters within these ranges and calculated resulting C:N ratios in a zero-dimensional setup. The range in the C:N ratio for each of the ranges in the parameter values is given in the last column.

there was no vertical structure, we could not vary the extinction depth d and the detritus sinking velocity w_S.

[13] In Table 2, we have summarized the standard parameter values, the chosen parameter ranges, and the resulting ranges in the C:N ratio. It appears that the predictions with respect to the C:N ratio are most sensitive to the saturation light flux $J_{L,FK}$ and the maximum C uptake rate $j_{EC,Am}$, i.e., to the parameters that determine the photosynthesis rate.

2.3. Initial Conditions

[14] The initial conditions for the biological fields were determined by a simulation of the PINC model in a one-dimensional setup (as in work by *Omta et al.* [2006]) with vertical transports as a consequence of only diffusion ($D_V = 1.0 \times 10^{-5}$ m^2 s^{-1}) and sinking of detritus. The simulation was run, until an equilibrium between sinking of organic detritus and upward downgradient transport of DIC and DIN had been reached after 3000 simulation years. The DIC and DIN profiles are shown in Figure 2. As a consequence of sinking of organic material and remineralization, both the DIC and DIN concentrations increase with depth.

[15] To define the initial eddy, we first choose the background temperature stratification as *Molemaker and Dijkstra* [2000]

$$T_b(z) = T_0 + T_1 e^{\frac{z}{z_b}}, \tag{9}$$

where z_b is the vertical temperature decay depth ($-H < z < 0$). In this way, the vertical temperature difference between top and bottom is given by $\Delta T = T_1(1 - e^{-\frac{H}{z_b}})$. Next, we superpose an eddy temperature field on this background temperature field defined by

$$T_e(r,z) = -\Delta T_e e^{-\left(\frac{r}{r_0}\right)^6} e^{\frac{z}{z_e}}, \tag{10}$$

where $r = ((x - L/2)^2 + (y - L/2)^2)^{1/2}$ is the distance from the center of the domain, ΔT_e the maximum temperature difference between the background temperature distribution and the temperature-distribution-with-eddy, r_0 the horizontal eddy radius, and z_e defines the vertical decay scale. The values of these stratification parameters are given in Appendix A, along with the values of the other

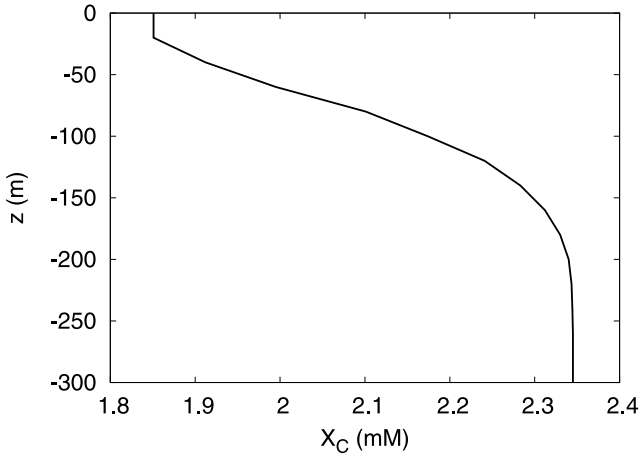

Figure 2a. Initial vertical profile of DIC throughout the upper 300 m of the domain.

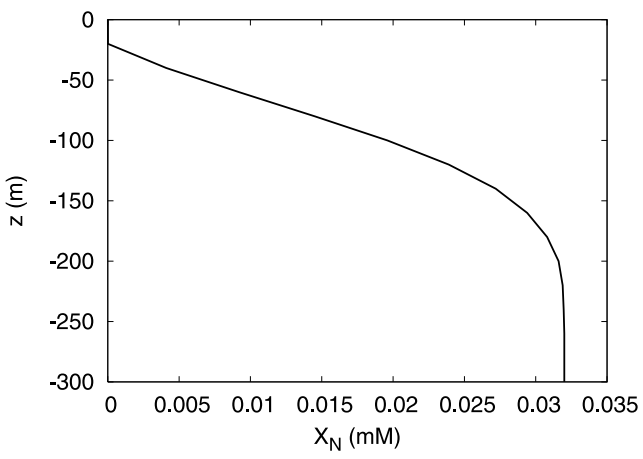

Figure 2b. Initial vertical profile of DIN throughout the upper 300 m of the domain.

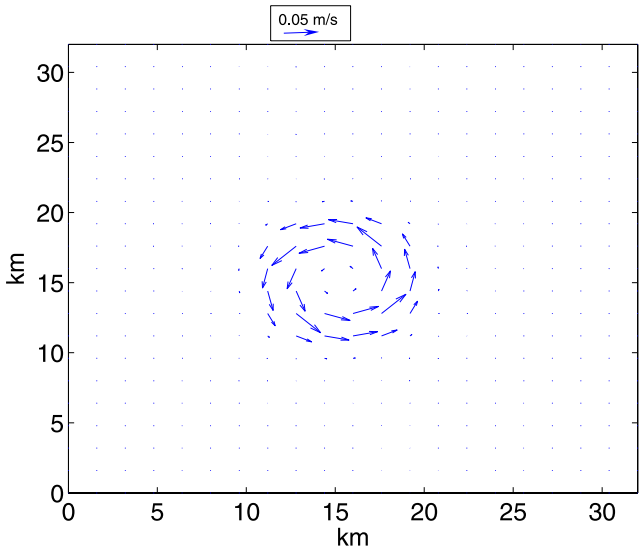

Figure 3. Vector plot of the initial horizontal velocity distribution of the eddy 50 m below the surface. The amplitude of this velocity field decays with depth, and the initial vertical velocity is equal to zero everywhere.

parameters of the hydrodynamic model. By writing the momentum balance (2) in cylindrical coordinates (as in, for example, work by *Molemaker and Dijkstra* [2000]) and assuming hydrostatic and cyclo-geostrophic equilibrium, we find the flow field

$$u = 0; v = \frac{rf_0}{2}\left(\sqrt{1 - \frac{4\alpha g}{rf_0^2}\int_{-H}^{z}\frac{\partial T_e}{\partial r}dz'} - 1\right); w = 0, \quad (11)$$

with u the radial velocity, v the azimuthal velocity, and w the vertical velocity. For the simulations, we have chosen T_1 = 3K, z_b = 0.4 km, z_e = 0.25 km, ΔT_e = 1.8K and r_0 = 4 km. The initial horizontal velocity field at 20 m depth is plotted in Figure 3.

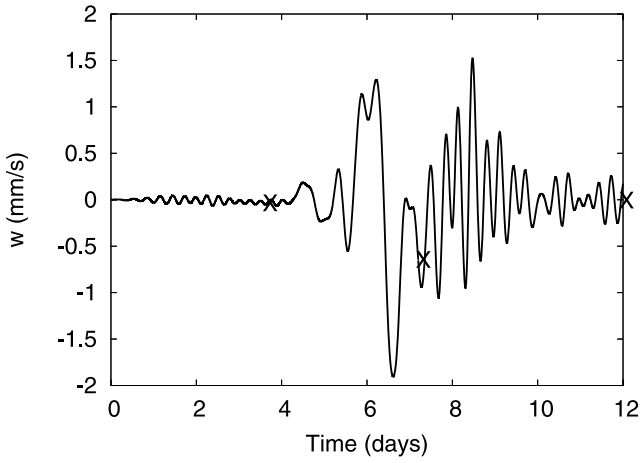

Figure 4. Vertical velocity as a function of time in the center of the eddy 50 m below the surface; the crosses indicate the times at which the horizontal cross sections are plotted in subsequent figures.

[16] Above, we have constructed an initial distribution of the biological tracers and an initial flow field separately. Together, these initial conditions form an equilibrium solution of the full coupled model, because the cyclo-geostrophic flow is in equilibrium and the biological tracer distributions are also in equilibrium, as long as there is no vertical flow. However, this equilibrium is unstable: the cyclo-geostrophic flow is susceptible to baroclinic instability that generates vertical flow which in turn disturbs the biological fields.

3. Results

[17] We have run the coupled model at a horizontal resolution of 160 m and a vertical resolution of 20 m. Our time step was equal to 75 seconds. From the initial conditions, the model was run over a time interval of about 12 days. As perturbations associated with baroclinic instability rapidly grow in time, an oscillatory flow results after about 1 day. The period of the oscillatory signal, seen in a plot of the vertical velocity at a specific gridpoint just below the surface at the eddy center (Figure 4) is about 0.7 days. In contrast to the eddy in the work by *Molemaker and Dijkstra* [2000], the initial eddy is unstable without surface cooling, because of the larger horizontal gradients in the density structure.

3.1. Temporal-Spatial Structures

[18] Just as in work by *Molemaker and Dijkstra* [2000], an azimuthal wave number m = 4 pattern, the most unstable eigenmode, grows in time and the anomalies rotate counterclockwise. The spatial patterns of the vertical velocity w and the nutrient distribution X_N at 20 m depth after 3.6 days are plotted in Figures 5a and 5b. The four-lobe flow pattern has already developed by then (Figure 5a). At the locations of maximum upwelling, X_N has the highest values (more than 10 μM, see Figure 5b). The biomass concentration is still very low everywhere. After 7.2 days, the lobes have started to separate themselves from the parent eddy. This is clearly visible in the spatial pattern of w and X_N (Figures 6a and 6b). Because of the high nutrient

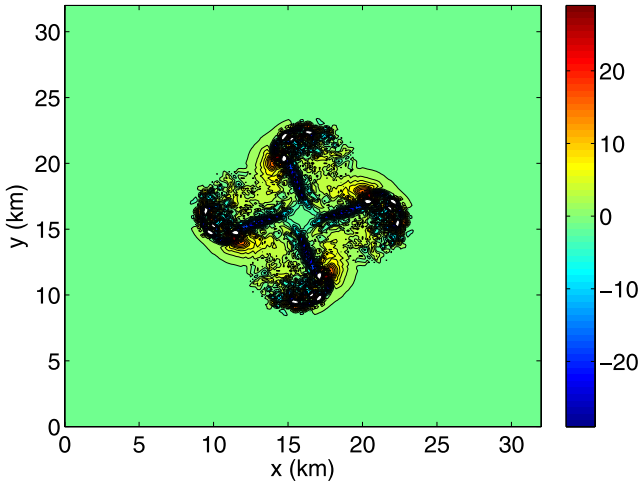

Figure 5a. Cross section of the vertical velocity distribution. Values are in 10^{-4} m/s. Positive numbers indicate upwelling, and negative numbers indicate downwelling.

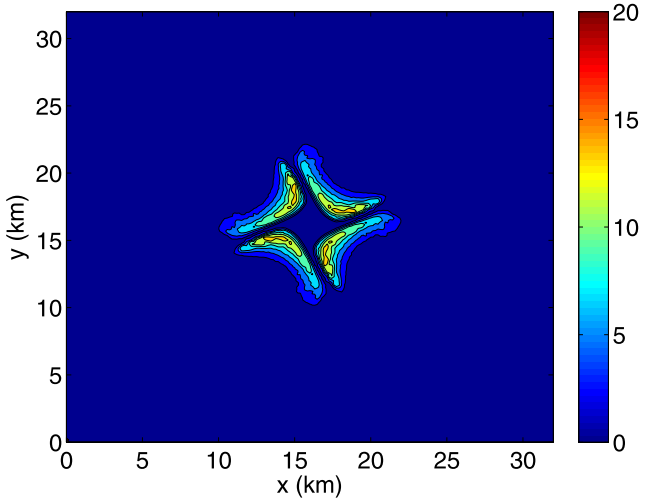

Figure 5b. Cross section of the X_N distribution; values are in μM.

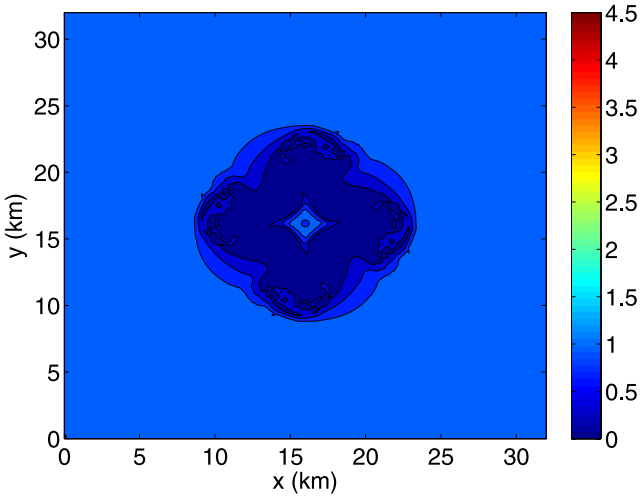

Figure 5d. Cross section of the carbon reserve concentration; values are in μM.

concentration in the upwelling regions, the algae can grow at maximum rate and after 7.2 days, the upwelled water has a high biomass concentration (1–5 μM, see Figures 6c–6e). The distribution of biomass shows a marked fine structure. The highest biomass concentrations (around 5 μM) are found in patches at the edges of the lobes. Around the central eddy, the four-lobe structure is visible in the form of four ribbons of high biomass. After 12 days, the lobes have moved nearly to the boundary of the domain (Figure 7); they may start to be affected by their mirror images because of the periodic boundary conditions. Therefore we have ended the simulation at this point in time. The inner eddy appears to undergo again an instability associated with an $m = 4$ mode, while the lobes seem to become unstable to an $m = 2$ mode (Figure 7a). The $m = 4$ spatial structure can be seen in the nutrient and biomass distributions in and around the central eddy (Figures 7b through 7e), but the amplitudes in the lobes are too weak to clearly distinguish the $m = 2$ structure.

[19] The highest structural biomass concentrations (more than 10 μM) are found in 'horseshoes' at the outer edges of the lobes (Figure 7) which can be explained by considering the impact of vertical mixing on algal growth. Vertical mixing brings DIN to the surface, thus promoting primary production. However, if the DIN concentration exceeds a certain value (in our simulation about 0.5 μM, because the saturation constant for nitrogen uptake K_N is equal to 0.1 μM), extra nitrogen does not promote algal growth anymore because of saturation. On the other hand, vertical mixing brings algae from the euphotic zone (i.e., the well-lit upper 50 m) into deeper water where the algae are not able to survive by lack of light. If the vertical mixing exceeds a critical value, then an algal population will even go extinct, as was pointed out by *Huisman et al.* [1999]. Hence, within the region where $X_N > 0.5$ μM, the highest net biomass increase rate is where the effective vertical mixing is minimal. In Figure 8, we show the 0.5 μM contour of X_N after 7.2 days. A comparison with Figure 6a shows that

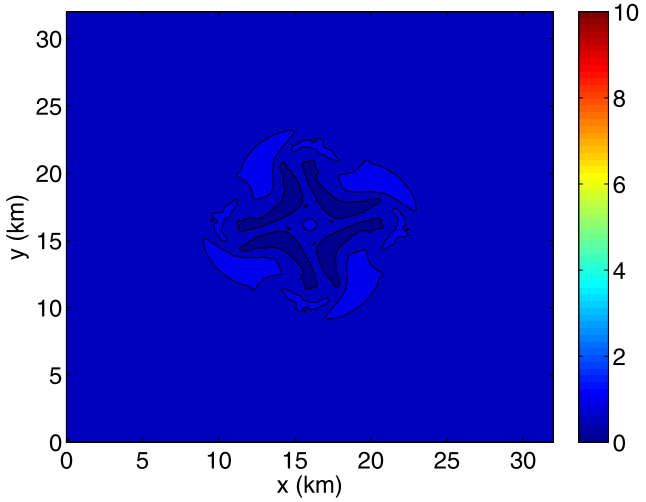

Figure 5c. Cross section of the structural volume distribution; values are in μM.

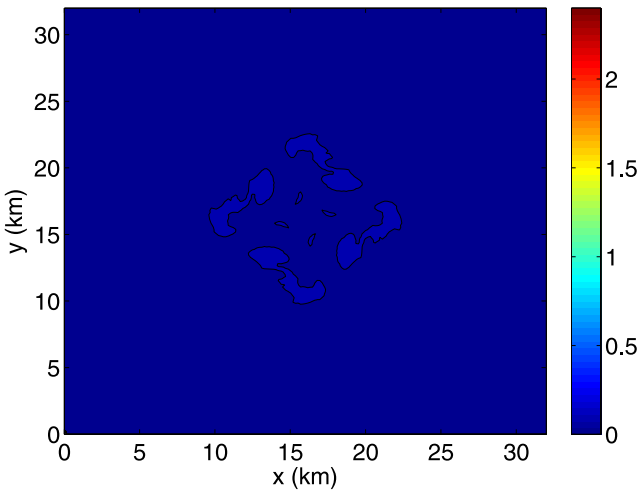

Figure 5e. Cross section of the nitrogen reserve concentration; values are in μM.

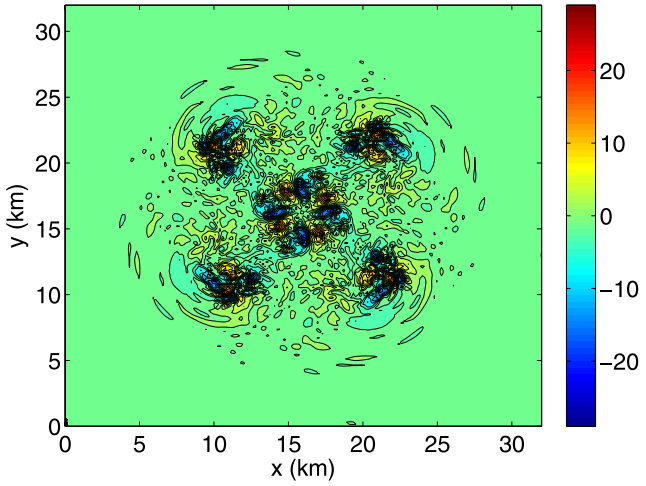

Figure 6a. Cross section of the vertical velocity distribution; values are in 10^{-4} m/s. Positive numbers indicate upwelling, and negative numbers indicate downwelling.

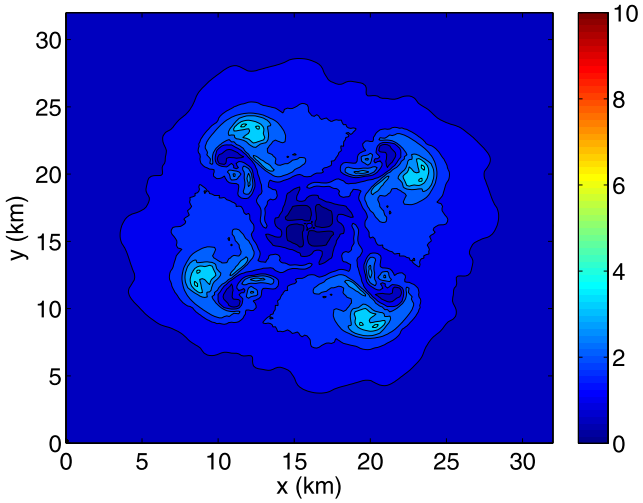

Figure 6c. Cross section of the X_V distribution; values are in μM.

along this contour, there is relatively little vertical mixing. Along the contour, the conditions are optimal for the algae: the nitrogen concentration is high enough to achieve a maximal growth rate, but there is relatively little vertical mixing. On the rear sides of the lobes, there are four small regions with $X_N < 0.5$ μM. Here the algae have already largely depleted the nitrogen. This does not immediately affect the growth rate, because the phytoplankton uses up its nitrogen reserve. This, however, has a dramatic effect on the nitrogen reserve concentration X_{EN}: after 12 simulation days, the X_{EN} concentration is extremely low on the rear sides of the lobes (see Figure 7e).

[20] Newly upwelled water has a low biomass concentration but a high nutrient concentration and it takes some time before the nutrients have been converted into biomass. Upward flow correlates with low (structural) biomass concentrations, as can be seen in Figure 9, where we show $\langle wX_V \rangle = \int wX_V dA$ (i.e., the horizontally integrated value of the product of the vertical velocity w and the structural biomass concentration X_V) as a function of depth at various times. At all times, $\langle wX_V \rangle$ is negative throughout the upper 150 m of the domain. This does not only indicate that there is little biomass at upwelling places and that there is a lot of biomass at downwelling sites, but also that there exists a net downward advective transport of structural biomass from the upper 150 m of the domain into deeper waters.

3.2. Soft-Tissue Pump

[21] Using the results of the simulation described in the previous subsection, we computed horizontally averaged values of the C:N ratio of the organic material and the surface nitrogen concentration. We are specifically interested in these two quantities, because they determine the strength of the soft-tissue carbon pump.

[22] The initial C:N ratio of detritus (computed from the initial state) is larger than 25 in the upper 30 m of the domain and around 13 in the deeper waters (Figure 10a). Over the following 7.2 days, the values decrease to around

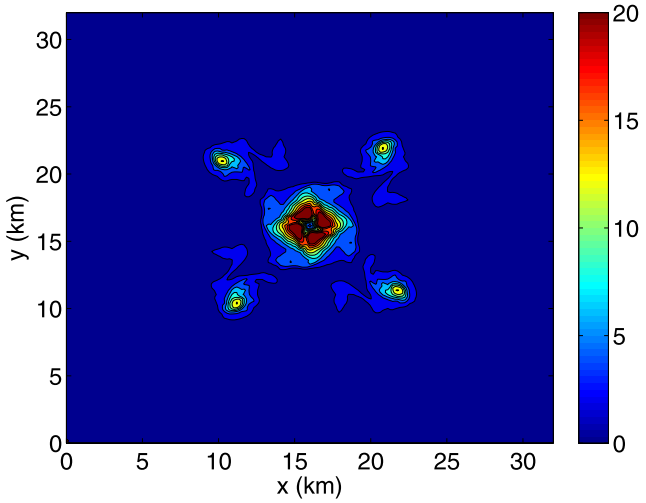

Figure 6b. Cross section of the X_N distribution; values are in μM.

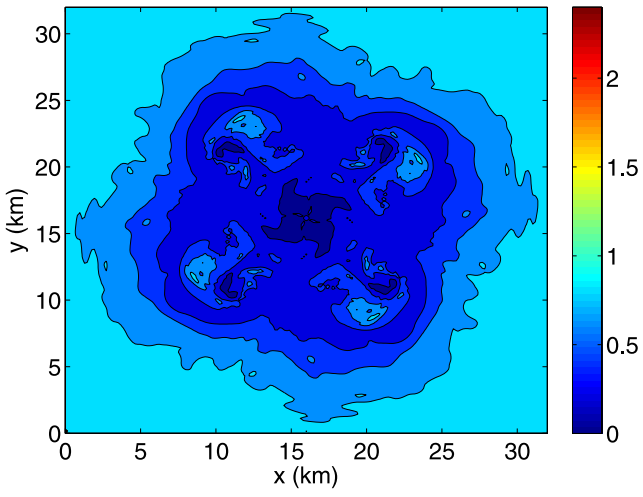

Figure 6d. Cross section of the X_{EC}; values are in μM.

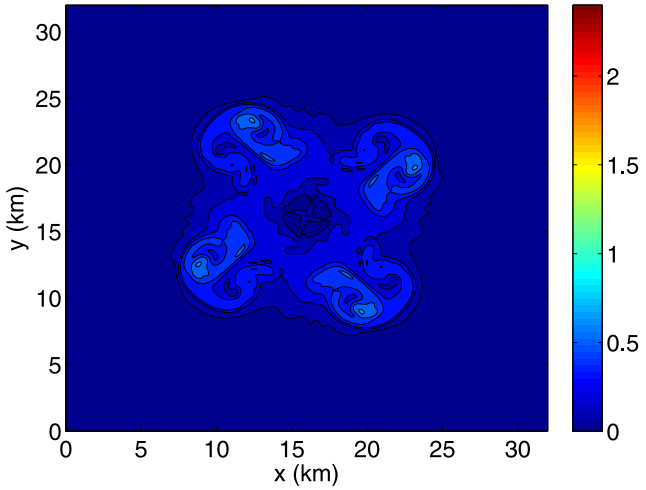

Figure 6e. Cross section of X_{EN}; values are in μM.

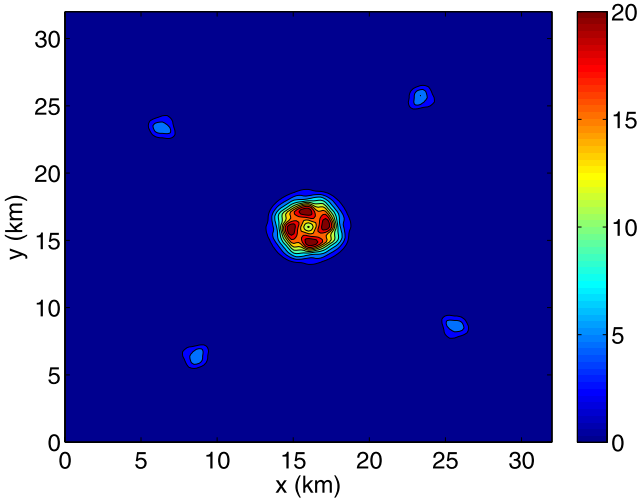

Figure 7b. Cross section of the X_N distribution; values are in μM.

12 everywhere in the upper 150 m. Below a depth of 10 m, there is a further decrease of the C:N ratio between 7.2 and 12 days after the start of the simulation. Over the entire simulation, the C:N ratio decreases by 20–50% throughout the upper 150 m.

[23] The overall decrease of the C:N ratio can be explained, if one considers the vertical transports induced by the eddy. Roughly, the C:N ratio is determined by the ratio of the uptake rates of carbon and nitrogen. If the uptake of carbon is faster than the uptake of nitrogen, then the organisms build up a large carbohydrate reserve. Similarly, they will build a large nitrogen reserve, when the uptake of nitrogen is relatively fast. The vertical transport induced by the eddy leads to an increasing DIN concentration at the surface. This, in turn, leads to an enhanced uptake of nitrogen per mole of structural biomass, while the uptake of carbon per mole of structural biomass remains approximately the same. The biological mechanism behind this is that higher nitrogen concentrations promote uptake of nitrogen, but not uptake of carbon. Uptake of carbon proceeds through photosynthesis and therefore carbon uptake is in general not stimulated by nutrients but by light.

[24] In Table 3, we show the DIC uptake (kmol/s), the DIN uptake (kmol/s), both integrated over the entire domain, and $\int X_V dV$, i.e., the total amount of structural biomass within the domain (in Mmol) at various times. There is a strong increase in the integrated uptake of both DIC and DIN with time. Nevertheless, the total uptake of DIN increases by about a factor 12 over the twelve days, while the total uptake of DIC only increases by approximately a factor 7. Because the total amount of biomass increases by about a factor 6, the DIC uptake per mol of biomass remains approximately the same, while the DIN uptake per mol of biomass increases.

[25] The soft-tissue carbon pump does not only depend on the C:N ratio, but also on the fraction of the upwelling nutrients that is actually consumed by biota. Therefore we have also analyzed the development of the DIN distribution. In Figure 10b, we show the horizontally averaged difference

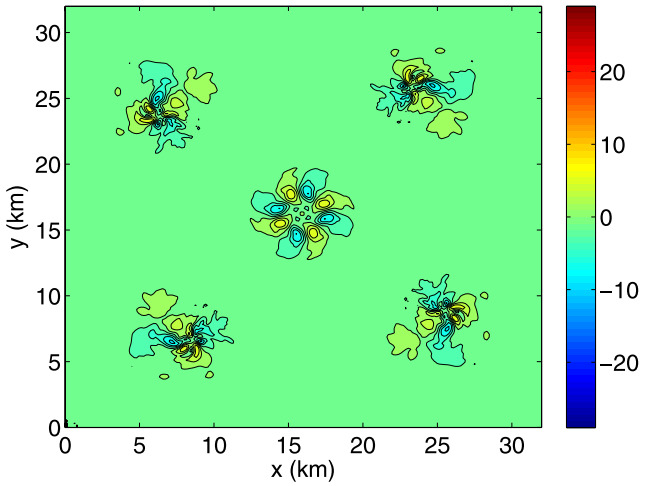

Figure 7a. Cross section of the vertical velocity distribution; values are in 10^{-4} m/s. Positive numbers indicate upwelling, and negative numbers indicate downwelling.

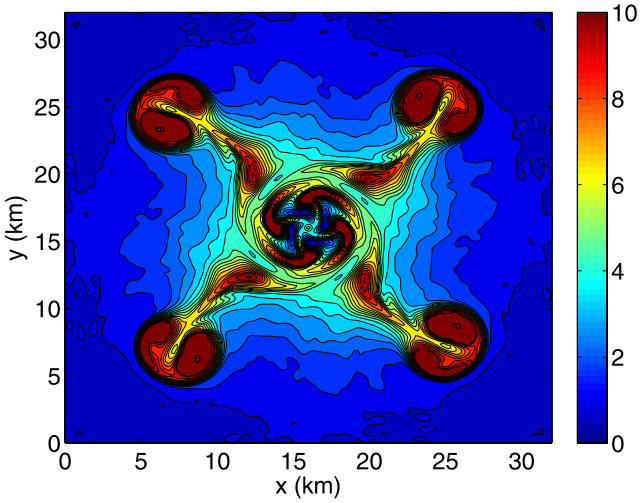

Figure 7c. Cross section of the X_V distribution; values are in μM.

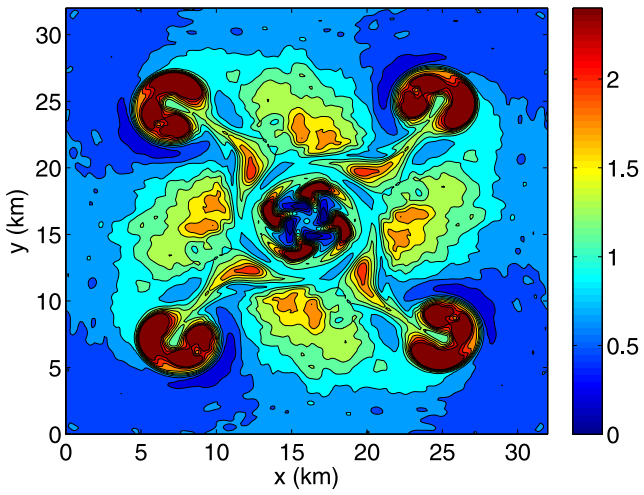

Figure 7d. Cross section of X_{EC}; values are in μM.

between the DIN concentration and the initial DIN concentration at various times as a function of depth. This difference is positive during our simulation (see Figure 10b); that is, the surface DIN concentration slightly increases. This means that not all of the upwelled DIN is consumed. Thus the increase of the surface DIN concentration implies a weakening of the soft-tissue carbon pump, as we discuss in more detail in section 4. Hence the changes in both the plankton stoichiometry and the nutrient utilization lead to a weakening of the soft-tissue carbon pump.

[26] We have also analyzed the actual carbon transports associated with the sinking of organic material. In Figure 11, we show the horizontally integrated vertical sinking flux of X_{DC} after 0 and 12 days. Near the surface, there is a strong increase in the downward sinking flux. However, during the simulation, there is also a strong increase in the upward transport of DIC toward the surface. Hence there is a competition between an increase in the upwelling of inorganic carbon and an increase in the sinking flux of organic carbon. Which one of these two processes is stronger, is eventually determined by the nutrient utilization and the

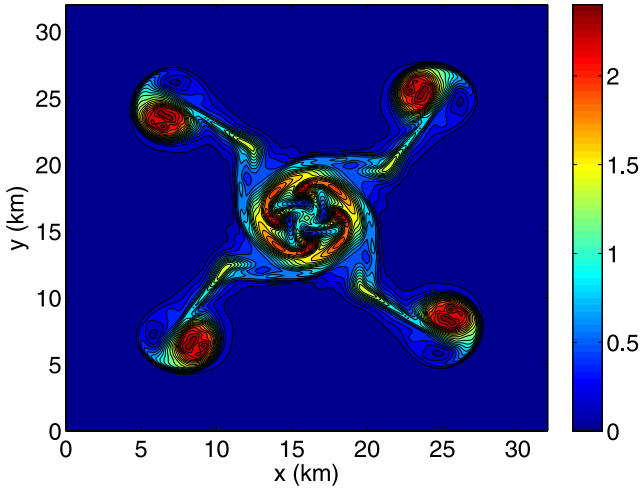

Figure 7e. Cross section of X_{EN}; values are in μM.

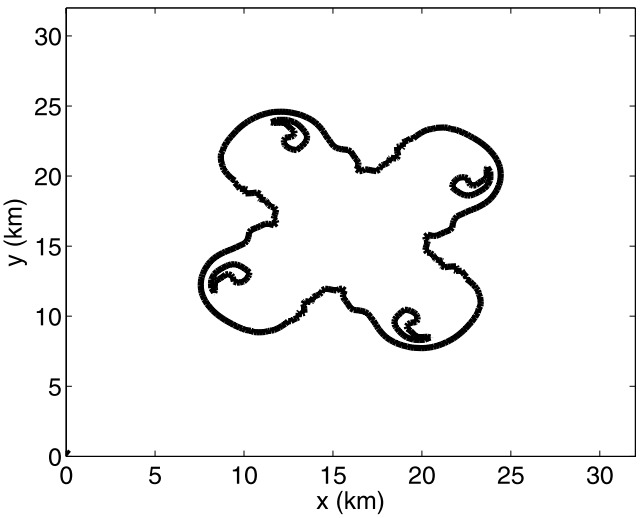

Figure 8. Iso-curve of X_N at 20 m depth after 7.2 days. The black curve connects the points where X_N = 0.5 μM. Hence it separates the nitrogen-limited from the nitrogen-replete regions.

C:N ratio of the sinking organic material, as we discuss in section 4.

3.3. Sensitivity

[27] Unfortunately, a proper sensitivity analysis is extremely time demanding and difficult, since one single simulation with our coupled model already takes about 100 CPU hours on a HP-DS 25 (1 GHz) and the PINC model organism alone has 13 parameters. As we mentioned in section 2.2, the predictions of the biological model seem to be most sensitive to the values of the photosynthesis parameters $J_{L,FK}$ and $j_{E_C,Am}$.

[28] We first have varied $J_{L,FK}$ over two orders of magnitude in the coupled setup. Again, the initial conditions for the biological fields were determined by a simulation of

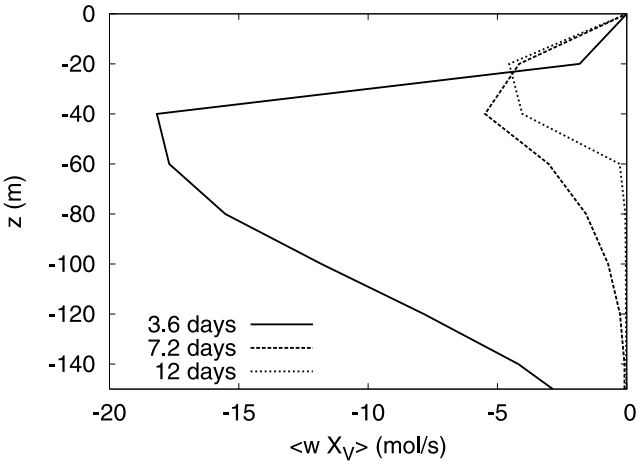

Figure 9. Horizontally integrated value of the product of the vertical velocity w and the structural biomass concentration X_V. The negative values indicate that w and X_V are anticorrelated and that there exists a net downward advective transport of structural biomass.

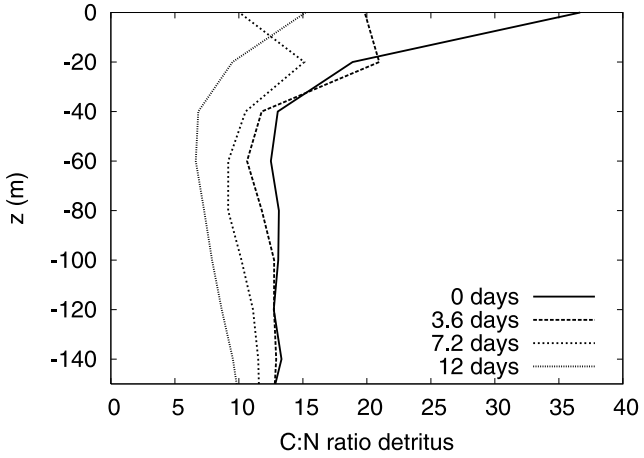

Figure 10a. Horizontally averaged C:N ratio of detritus as a function of depth at different times.

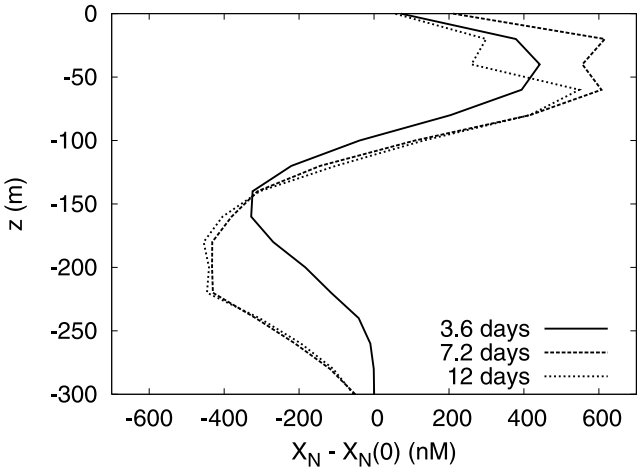

Figure 10b. Horizontally averaged difference between nitrogen concentration (X_N) and initial nitrogen concentration ($X_N(0)$) as a function of depth at different times.

the PINC model in a one-dimensional setup with vertical transports as a consequence of diffusion and sinking of detritus, but without vertical transports caused by flow advection. The flow development is the same as in the experiments described in sections 3.1 and 3.2. The horizontally averaged C:N ratios as a function of depth at different times are shown in Figure 12. Although the actual C:N ratios vary a lot, the main trend remains the same: the flow development due to the baroclinic instability of the eddy leads to a lower C:N ratio of the sinking detritus.

[29] For the standard simulation, with $j_{E_C,Am} = 2.5$ mol/(m^2 d), we have $n_{N,V} = 0.1$ which means that the C:N ratio of structural biomass equals 10 and $\frac{j_{E_N,Am}}{j_{E_C,Am}} = 0.1$, implying that the C:N ratio of uptake under conditions of abundant light and nutrients equals 10 also. Given the classical Redfield ratio, these C:N ratios may seem a bit on the high side. To investigate the influence of this parameter choice, we have performed a simulation with the full coupled model with $j_{E_C,Am} = 1.25$ mol/(m^2 d) giving $n_{N,V} = \frac{j_{E_N,Am}}{j_{E_C,Am}} = 0.2$ (i.e., the C:N of structural mass and of nutrient- and light-replete uptake equals 5). The horizontally averaged C:N ratios as a function of depth at different times are shown in Figure 13. Again, the actual C:N ratios are quite sensitive to the parameter value, but the main trend remains the same: the mixing resulting from baroclinic instability of the eddy leads to a decrease of the C:N ratio of the sinking detritus.

4. Discussion and Conclusions

[30] We have simulated a phytoplankton population within a submesoscale eddy. Within this eddy, baroclinic instability caused a vertical circulation pattern, leading to a higher surface DIN concentration and a lower C:N ratio of the sinking detritus.

[31] Before the baroclinic instability sets in, there exists a small diffusive transport of DIN and DIC upward from the deep sea into the euphotic zone. There the DIN and DIC are consumed by the biota in the stoichiometric ratio in which they were just transported upward and eventually, the C and N are returned to depth by sinking. Hence, there is no net upward or downward transport of C and N in this equilibrium situation. As the baroclinic instability sets in, more C and N are transported upward from the deep sea into the euphotic zone. The surface DIN concentration increases throughout the simulation and this can only be the case, if the upward transport of DIN is higher than the consumption of DIN by the biota. If the C:N ratio of the consumption by biota remains the same as before the instability set in, then not all of the DIC that is transported upward is consumed. This means that there is a net upward transport of C from the deep sea to the surface. The decrease of the C:N ratio of

Table 3. Total Uptake of DIC and DIN and Total Amount of Structural Biomass Within the Domain at Various Times

Time, days	DIC Uptake, kmol/s	DIN Uptake, kmol/s	$\int X_V dV$, Mmol
0	0.20	0.013	22
3.6	0.26	0.020	23
7.2	0.49	0.047	40
12	1.48	0.15	120

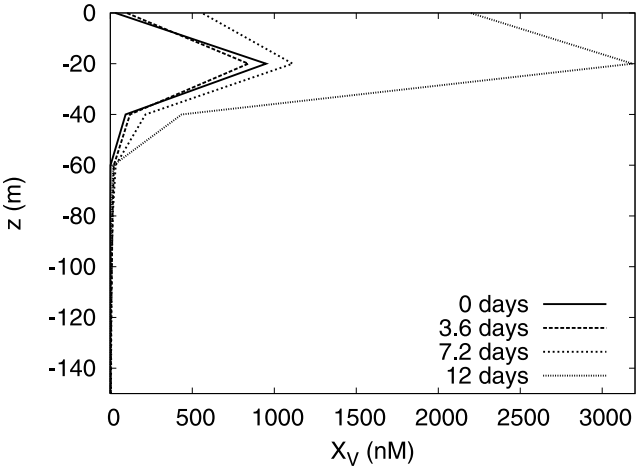

Figure 10c. Horizontally averaged structural biomass concentration (X_V) as a function of depth at different times.

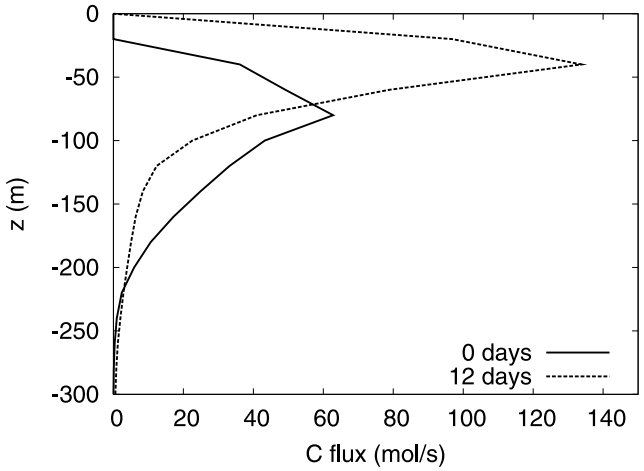

Figure 11. Horizontally averaged sinking flux of X_{DC} after 0 and 12 days throughout the upper 300 m.

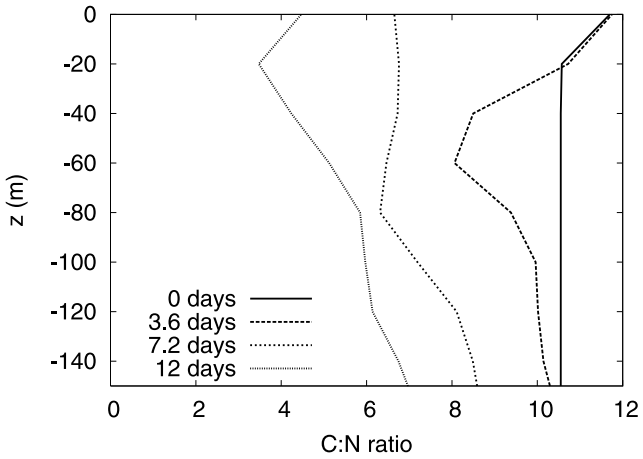

Figure 12b. Horizontally averaged C:N ratio of detritus as a function of depth at different times for $J_{L,FK}$ = 250 mol/(m^2 d).

the biota during the eddy instability increases the imbalance between upwelling and consumption of DIC. Hence both the increase in the surface DIN concentration and the decrease of the C:N ratio of the biota imply a net upward transport of DIC which means a weakening of the soft-tissue carbon pump.

[32] At the end of the simulation, biomass concentrations are relatively high in all the regions where upwelling has been taking place, i.e., in and around the eddy center and the lobes, but there is still relatively little biomass at locations where upwelling is taking place. Upwelling brings water with a high nitrogen and a low biomass concentration to the surface. In this newly upwelled water, an algal bloom develops because of the high nitrogen concentration. However, there exists a time delay between the upwelling and the emergence of the bloom, because the algae need time to assimilate the new nitrogen into their nitrogen reserve and they also need time to mobilize nitrogen from their reserve for growth. Therefore only water that has upwelled more than a few days earlier has a relatively high biomass concentration. Previous simulations of plankton growth in an unstable jet also demonstrated that biomass was low in upwelling regions, increasing with the time the water had been upwelled [*Spall and Richards*, 2000]. Another interesting feature is the occurrence of patches with very high biomass concentrations at the outer edges of the lobes. These patches neither correspond to areas of strong vertical mixing nor to any particular flow feature. The high biomass concentrations are found here because the conditions for plankton growth are optimal: a high nitrogen concentration combined with a relatively low vertical mixing.

[33] We did not include self-shading into our PINC model, because it is only important at extremely high plankton concentrations of more than 10^6 cells/mL. If self-shading is important, then the phytoplankton will become light-limited, once the biomass density becomes high. This can lead to a cessation of the net population growth, even if the nutrient concentration is still very high. Another consequence of this light limitation would be a decrease of the C:N ratio of the organisms, because the DIC uptake rate decreases under light-limitation, while the DIN uptake rate is unaffected. During the course of our simula-

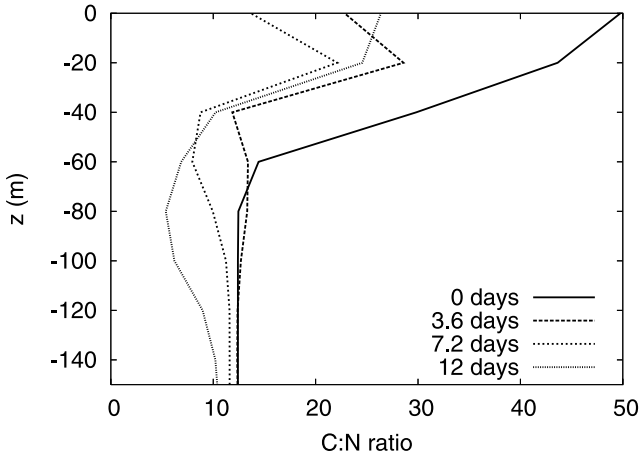

Figure 12a. Horizontally averaged C:N ratio of detritus as a function of depth at different times for $J_{L,FK}$ = 2.5 mol/(m^2 day).

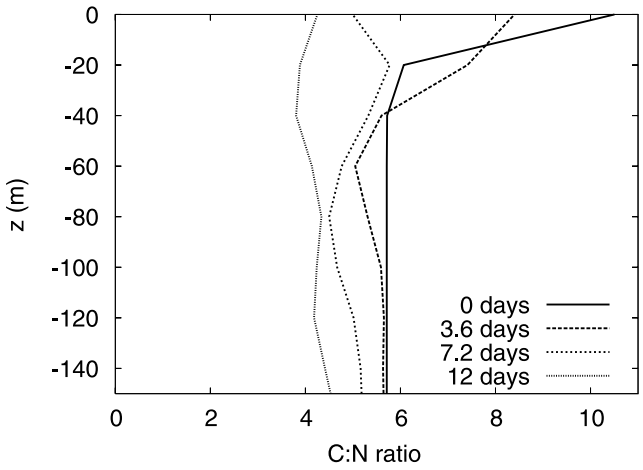

Figure 13. Horizontally averaged C:N ratio of detritus as a function of depth at different times for $n_{N,V}$ = 0.2.

Table 4. Model Organism Variables

Variable	Interpretation	Units
$J_{E_C,A}$	carbon assimilation	μM C/d
$J_{E_N,A}$	nitrogen assimilation	μM N/d
$J_{E_C,C}$	mobilized flux from C reserve	μM C/d
$J_{E_N,C}$	mobilized flux from N reserve	μM N/d
$J_{V,C}$	catabolic flux	μM C/d
$J_{E_C,R}$	rejected flux from C reserve	μM C/d
$J_{E_N,R}$	rejected flux from N reserve	μM N/d
μ	specific growth rate	d^{-1}
$J_{V,G}$	growth	μM C/d
$J_{D_C,A}$	flux of C into C-detritus	μM C/d
$J_{D_N,A}$	flux of N into N-detritus	μM N/d
X_C	DIC concentration	μM C
X_N	DIN concentration	μM N
X_V	biomass structure concentration	μM C
X_{E_C}	C-reserve concentration	μM C
X_{E_N}	N-reserve concentration	μM N
X_{DC}	C-detritus concentration	μM C
X_{DN}	N-detritus concentration	μM N

tion, the population density strongly increases in the region of the eddy and the lobes. Inclusion of self-shading could then lead to an extra decrease of the C:N ratio and to a relatively smaller plankton population. This smaller population will take up less DIN, even though the DIN uptake rate (per amount of structural biomass) is unaffected. Hence inclusion of self-shading would enhance the effects on the soft-tissue carbon pump, because of an extra decrease of the C:N ratio and a lower nutrient utilization.

[34] Various data sets [see, e.g., *Schneider et al.*, 2003] indicate that the C:N ratio of organic material slightly increases with depth which suggests that the remineralization depth of C is larger than the remineralization depth of N. Inclusion of this effect into our model would lead to a slightly different DIC (X_C) profile, with a decreased X_C concentration gradient near the surface and a higher X_C gradient in the deep. However, the results of our simulation would not change very much. The vertical transports would still result in a lower nutrient utilization and a lower C:N of the sinking material and hence in a weakening of the soft-tissue carbon pump.

[35] To our knowledge, there do not exist reliable observational estimates of vertical velocities associated with eddies of this particular scale. Our simulated vertical velocities are relatively high when compared to the vertical velocities observed in baroclinically unstable flow structures such as mesoscale fronts and jets [*Martin*, 2003].

[36] Our model predicts the C:N ratio of algae within a baroclinically unstable (sub)mesoscale eddy to be relatively low compared to the C:N ratio of algae outside such an eddy. We only know of one observational study of the C:N:P ratio of the uptake by algae from a mesoscale eddy [*Rees et al.*, 2001]. The measurements indicated a relatively high C:N ratio. However, *Rees et al.* [2001] did not measure the C:N ratio of uptake by algae outside the eddy. Therefore we do not know whether the C:N ratio of algal uptake was actually higher or lower within the eddy compared to its surroundings.

[37] Unfortunately, it is not clear whether variations in the stoichiometry of the phytoplankton growing at the surface of the ocean translate into variations in the stoichiometry of the sinking organic material. In fact, the composition of the sinking material seems to be pretty constant across the world ocean [*Schneider et al.*, 2003], even though large variations in the stoichiometry of the consumption of carbon, nitrogen, and phosphorus by phytoplankton have been observed at the ocean surface [e.g., *Sambrotto et al.*, 1993; *Arrigo et al.*, 1999]. This could suggest that the sinking organic material is very rich in one particular chemical compound while all the other organic compounds are largely remineralized within the euphotic zone. From this viewpoint, it is interesting that the C:N ratio of the sinking organic matter is on average very close to the C:N ratio of chitin (which is equal to 8), a compound that forms the exoskeleton of zooplankton, crustaceans, krill, etc. [*Jeuniot and Voss-Foucart*, 1991] It is unfortunate that the composition of POM is usually only given in terms of elements and not in terms of chemical compounds. We hope that such measurements will be reported in the near future.

Appendix A: PINC Model Details

[38] Here we provide a detailed description of the PINC model and the explicit formulation of the fluxes F_i, $i = 1, \ldots, 7$ in (7).

[39] The PINC organism produces nitrogen reserve (X_{E_N}) by assimilating DIN (X_N) according to Holling type II kinetics [*Holling*, 1959],

$$J_{E_N,A} = j_{E_N,Am}\frac{X_V}{1+x_N^{-1}}, \quad x_N = \frac{X_N}{K_N}, \tag{A1}$$

in which $j_{E_N,Am}$ denotes the specific maximum nutrient assimilation rate, X_N the external nutrient concentration, and K_N the nutrient half-saturation concentration.

[40] Carbohydrate reserve (X_{E_C}) is produced by assimilating DIC (X_C) through photosynthesis using light according to Synthesizing Unit (SU) [*Kooijman*, 2000] kinetics,

$$J_{E_C,A} = j_{E_C,Am}\frac{X_V}{1+x_C^{-1}+x_L^{-1}-(x_C+x_L)^{-1}},$$
$$x_C = \frac{X_C}{K_C}, x_L = \frac{J_{L,F}}{J_{L,FK}}, \tag{A2}$$

in which X_V denotes structural biomass, $j_{E_C,Am}$ the specific maximum rate of photosynthesis, X_C the external CO_2 concentration, K_C the CO_2 half-saturation concentration, $J_{L,F}$ the external light intensity, and $J_{L,FK}$ the half-saturation light intensity; x_C and x_L can be thought of as scaled availability of nutrient and light, respectively.

[41] From both the reserves, material is mobilized to build structural biomass with a fixed stoichiometric composition. The reserves become available for catabolic processes at rates

$$J_{E_C,C} = (k_E - \mu)X_{E_C}, \tag{A3a}$$

$$J_{E_N,C} = (k_E - \mu)X_{E_N},, \tag{A3b}$$

with k_E denoting the rate of reserve mobilization, and μ denoting the specific growth rate. The kinetics of (A3a) and (A3b) is derived by *Kooijman* [2000]; it can be shown to

simplify to Droop kinetics under particular conditions. Mobilized reserves are used to produce new structural biomass, according to a two-substrate synthesizing unit transformation [*Kooijman*, 2000],

$$J_{V,C} = \frac{1}{\left(\frac{J_{E_C,C}}{y_{E_C,V}}\right)^{-1} + \left(\frac{J_{E_N,C}}{y_{E_N,V}}\right)^{-1} - \left(\frac{J_{E_C,C}}{y_{E_C,V}} + \frac{J_{E_N,C}}{y_{E_N,V}}\right)^{-1}}, \tag{A4}$$

with $y_{E_C,V}$ (>1) denoting the amount of organic carbon reserve needed to synthesize one unit of structure, and $y_{E_N,V}$ ($>n_{N,V}$) denoting the amount of nutrient reserve needed to synthesist one unit of structure. There is an overhead of $J_{V,C}(y_{E_C,V} - 1)$ units of carbon reserve per time, and $J_{V,C}(y_{E_N,V} - n_{N,V})$ of nitrogen reserve per time, with $n_{N,V}$ denoting the nitrogen content of one unit of structural mass. The overhead is exudated into the inorganic matter pools. The production rate follows from the rate of reserve mobilization, and is therefore restricted by the maximum reserve density; for this reason, we refrain from additionally imposing a maximum production rate as in (A2).

[42] The rate of structural biomass production is simultaneously limited by the rate of mobilization of both reserves. This implies that mobilized reserve is never fully used in structure synthesis (though complete use of one resource is approached when the other is abundant). The part of the mobilized reserve rejected by the process of structure synthesis is given by

$$J_{E_C,R} = J_{E_C,C} - y_{E_C,V} J_{V,C}, \tag{A5a}$$

$$J_{E_N,R} = J_{E_N,C} - y_{E_N,V} J_{V,C}. \tag{A5b}$$

We have implemented the processes of storage and exudation into the model by defining the parameter κ; a fixed fraction $0 < \kappa < 1$ of the rejected flux returns to the reserves, whereas the remaining fraction $1 - \kappa$ is exudated. For the sake of simplicity, we take κ equal for both reserves. Additionally, exudated compounds are assumed to be remineralized instantaneously; they thus contribute to the external CO_2 and nutrient pools.

[43] Structural biomass, not reserves, requires maintenance, which is implemented as a fixed turnover rate k_M of structural biomass that returns to the dissolved inorganic matter pools. By diminishing the rate of structural mass synthesis with this turnover, we arrive at the net growth rate

$$J_{V,G} = J_{V,C} - k_M X_V, \tag{A6}$$

from which we can derive the specific growth rate

$$\mu = J_{V,G}/X_V. \tag{A7}$$

Because of the 'weak homeostasis' discussed by *Kooijman* [2000], the righthand side of (A7) is again a function of μ through the rates of reserve mobilization (A3a) and (A3b). By rearranging terms one can obtain an explicit expression for μ. Biomass (i.e., X_V, X_{E_C}, and X_{E_N}) turns into detritus at a death rate h_V. Because we are interested in the C:N ratio of this detritus, it is divided into a carbon component (X_{DC}) and a nitrogen component (X_{DN}). To close the carbon cycle, we impose a simple constant turnover of detritus h_D. This might be interpreted as remineralization of detritus by some constant background population of bacteria.

[44] With the parameters and variables as defined in Tables 2 and 4, the dynamic behavior of the full system is now described by

$$\frac{dX_C}{dt} = -J_{E_C,A} + (1-\kappa)J_{E_C,R} + (y_{E_C,V} - 1)J_{V,C} + X_V k_M + h_D X_{DC}, \tag{A8a}$$

$$\frac{dX_N}{dt} = -J_{E_N,A} + (1-\kappa)J_{E_N,R} + (y_{E_N,V} - n_{N,V})J_{V,C} + n_{N,V} X_V k_M + h_D X_{DN}, \tag{A8b}$$

$$\frac{dX_{E_C}}{dt} = J_{E_C,A} - J_{E_C,C} + \kappa J_{E_C,R} - h_V X_{E_C}, \tag{A8c}$$

$$\frac{dX_{E_N}}{dt} = J_{E_N,A} - J_{E_N,C} + \kappa J_{E_N,R} - h_V X_{E_N}, \tag{A8d}$$

$$\frac{dX_V}{dt} = X_V(\mu - h_V), \tag{A8e}$$

$$\frac{dX_{DC}}{dt} = h_V(X_V + X_{E_C}) - X_{DC} h_D, \tag{A8f}$$

$$\frac{dX_{DN}}{dt} = h_V(n_{N,V} X_V + X_{E_N}) - X_{DN} h_D. \tag{A8g}$$

[45] **Acknowledgments.** We would like to thank Jorn Bruggeman, Bob Kooi, Ben Sommeijer, and two anonymous reviewers for their careful reading of the manuscript and for their helpful comments. This work was financially supported through the Computational Life Science program of the Netherlands Organisation for Scientific Research (NWO) under grant 635.100.009.

References

Arrigo, K., D. Robinson, D. Worthen, R. Dunbar, G. DiTullio, M. Vanwoert, and M. Lizotte (1999), Phytoplankton community structure and the drawdown of nutrients and CO_2 in the Southern Ocean, *Science*, *283*, 365–367.

Broecker, W. S. (1982), Ocean geochemistry during glacial time, *Geochim. Cosmochim. Acta*, *46*, 1689–1705.

Dugdale, R. C., F. P. Wilkerson, and H. J. Minas (1995), The role of a silicate pump in driving new production, *Deep Sea Res., Part I*, *42*, 697–719.

Emerson, S., S. Mecking, and J. Abell (2001), The biological pump in the subtropical North Pacific Ocean: Nutrient sources, Redfield ratios, and recent changes, *Global Biogeochem. Cycles*, *15*, 535–554.

Geider, R. J., and J. la Roche (2002), Redfield revisited: Variability of C:N:P in marine microalgae and its biochemical basis, *Eur. J. Phycol.*, *37*, 1–17.

Healey, F. P. (1985), Interacting effects of light and nutrient limitation on the growth of synechococcus linearis (cyanophyceae), *J. Phycol.*, *21*, 134–146.

Holling, C. S. (1959), Some characteristics of simple types of predation and parasitism, *Can. Entomol.*, *91*, 385–398.

Huisman, J., P. van Oostveen, and F. J. Weissing (1999), Critical depth and critical turbulence: Two different mechanisms for the development of phytoplankton blooms, *Limnol. Oceanogr.*, *44*, 1781–1787.

Hundsdorfer, W., and J. G. Verwer (2003), *Numerical Solution of Time-Dependent Advection-Diffusion-Reaction Equations*, 1st ed., Springer, Berlin.

Jeuniot, C., and M. F. Voss-Foucart (1991), Chitin biomass and production in the marine environment, *Biochem. Syst. Ecol.*, *19*, 347–356.

Karl, D. M., K. M. Björkman, J. E. Dore, L. Fujieki, D. V. Hebel, T. Houlihan, R. M. Letelier, and L. M. Tupas (2002), Ecological nitrogen-to-phosphorus stoichiometry at station aloha, *Deep Sea Res., Part II*, *29*, 2074.

Kooijman, S. A. L. M. (2000), *Dynamic Energy and Mass Budgets in Biological Systems*, Cambridge Univ. Press, Cambridge, U.K.

Kooijman, S. A. L. M., H. A. Dijkstra, and B. W. Kooi (2002), Light-induced mass turnover in a mono-species community of mixotrophs, *J. Theor. Biol.*, *214*, 233–254.

Lévy, M., P. Klein, and A. M. Treguier (2001), Impacts of sub-mesoscale physics on phytoplankton production and subduction, *J. Mar. Res.*, *59*, 535–565.

Martin, A. P. (2003), Phytoplankton patchiness: The role of lateral stirring and mixing, *Prog. Oceanogr.*, *57*, 125–174.

Martin, A. P., and K. J. Richards (2001), Mechanisms for vertical nutrient transport within a north atlantic mesoscale eddy, *Deep Sea Res., Part II*, *48*, 757–773.

McGillicuddy, D. J., A. R. Robinson, D. A. Siegel, H. W. Jannasch, R. Johnson, T. D. Dickey, J. McNeil, A. F. Michaels, and A. H. Knap (1998), Influence of mesoscale eddies on new production in the Sargasso Sea, *Nature*, *394*, 263–266.

Molemaker, M. J., and H. A. Dijkstra (2000), Stability of a cold-core eddy in the presence of convection: Hydrostatic versus nonhydrostatic modeling, *J. Phys. Oceanogr.*, *30*, 475–494.

Okubo, A. (1971), Oceanic diffusion diagrams, *Deep Sea Res*, *18*, 789–802.

Omta, A. W., J. Bruggeman, S. A. L. M. Kooijman, and H. A. Dijkstra (2006), The biological carbon pump revisited: feedback mechanisms between climate and the Redfield ratio, *Geophys. Res. Lett.*, *33*, L14613, doi:10.1029/2006GL026213.

Oschlies, A., and V. Garçon (1998), Eddy-induced enhancement of primary production in a model of the North Atlantic Ocean, *Nature*, *394*, 266–269.

Rees, A. P., I. Joint, E. M. S. Woodward, and K. M. Donald (2001), Carbon, nitrogen and phosphorus budgets within a mesoscale eddy: Comparison of mass balance with in vitro determinations, *Deep Sea Res., Part II*, *48*, 859–872.

Sambrotto, R. N., et al. (1993), Elevated consumption of carbon relative to nitrogen in the surface ocean, *Nature*, *363*, 248–250.

Schneider, B., R. Schlitzer, G. Fischer, and E. M. Nöthig (2003), Depth-dependent elemental compositions of particulate organic matter (POM) in the ocean, *Global Biogeochem. Cycles*, *17*(2), 1032, doi:10.1029/2002GB001871.

Spall, S. A., and K. J. Richards (2000), A numerical model of mesoscale frontal instabilities and plankton dynamics: I. Model formulation and initial experiments, *Deep Sea Res., Part I*, *47*, 1261–1301.

Sterner, R. W., and J. J. Elser (2002), *Ecological Stoichiometry*, Princeton Univ. Press, Princeton, N. J.

Volk, T., and M. I. Hoffert (1985), Ocean carbon pumps: Analysis of relative strengths and efficiencies in ocean-driven atmospheric CO_2, in *The Carbon Cycle and Atmospheric CO_2: Natural Variations Archean to Present*, *Geophys. Monogr. Ser.*, vol. 32, edited by E. T. Sundquist and W. S. Broecker, pp. 99–110, AGU, Washington, D. C.

Wunsch, C., and R. Ferrari (2004), Vertical mixing, energy and the general circulation of the oceans, *Annu. Rev. Fluid Mech.*, *36*, 281–314.

H. Dijkstra, Institute for Marine and Atmospheric Research Utrecht (IMAU), Department of Physics and Astronomy, Universiteit Utrecht, Princetonplein 5, NL-3582 CC Utrecht, Netherlands.

B. Kooijman and A. W. Omta, Institute for Molecular Cell Biology, Faculty of Earth and Life Sciences, Vrije Universiteit, De Boelelaan 1081, NL-1081 HV Amsterdam, Netherlands. (anne.willem.omta@falw.vu.nl)